Acta Biomed 2018; Vol. 89, Supplement 1: 18-33 DOI: 10.23750/abm.v89i1-S.7008

Review

Magnetic Resonance Imaging correlates of benign and malignant alterations of the spinal bone marrow

Ferdinando Caranci[1], Enrico Tedeschi[2], Lorenzo Ugga[2], Alessandra D'Amico[2], Serena Schipani[1], Silvia Bartollino[1], Claudio Russo[1], Alessandra Splendiani[3], Francesco Briganti[2], Marcello Zappia[1], Mariarosa A.B. Melone[4], Carlo Masciocchi[3], Luca Brunese[1]

[1] Department of Medicine and Health Sciences "V. Tiberio", University of Molise, Campobasso, Italy; [2] Unit of Neuroradiology, Department of Advanced Biomedical Sciences, "Federico II" University, Naples, Italy; [3] Department of Biotechnologies and Applied Clinical Sciences, University of L'Aquila, L'Aquila, Italy; [4] Division of Neurology, Department of Clinical and Experimental Medicine and Surgery; Centro Interuniversitario per la Ricerca in Neuroscienze (CIRN), University of Campania "Luigi Vanvitelli", Naples, Italy

Summary. *Background and aim of the work:* Bone marrow (BM) abnormalities in the spine are a common, sometimes unexpected, finding on Magnetic Resonance Imaging (MRI), which is the most sensitive imaging modality to evaluate the marrow, and their interpretation can be difficult for the unexperienced radiologist. In this review, the MRI appearance of normal age-related BM changes, as well as the imaging features of benign and malignant diseases, are presented. *Discussion:* A large variety of BM signal alterations has been identified and described, including normal variants, BM reconversion, degenerative changes, infections, spondyloarthritis and osteonecrosis, trauma, neoplastic lesions (both primary or metastatic), post-radiation and chemotherapy sequelae. *Conclusions:* Knowledge of normal age-related BM appearance, normal variants and patterns of involvement in focal and diffuse bone diseases is essential, together with clinical and laboratory data, to narrow the list of the possible differential diagnoses. The radiologist should be familiar with these signal changes, as they can sometimes be discovered incidentally. In this context, it is equally important not to attribute pathological significance to benign alterations and to promptly detect signs of malignant diseases. (www.actabiomedica.it)

Key words: bone marrow, avascular necrosis, leukemia, lymphoma, magnetic resonance imaging, myelofibrosis, myeloma, osteomyelitis, osteonecrosis, spondyloarthritis

Introduction

The bone marrow (BM) is one of the largest organs of the human body, representing about 4% of the total body weight. Functionally, it serves as the primary site for hematopoiesis and as a major reticuloendothelial organ involved in immune responses (cellular and humoral) (1-5).

BM can be found in almost any bone that hosts spongy bone tissue, such as femur, ribs and vertebrae (above all in the durso-lumbar tract).

Thus, BM abnormalities in the spine are a common, sometimes unexpected, finding on Magnetic Resonance Imaging (MRI), which is the most sensitive imaging modality to evaluate the marrow, and their interpretation can be difficult for the unexperienced radiologist.

A large variety of BM signal alterations has been identified and includes normal variants, BM reconversion, neoplastic lesions (both primary or metastatic), radiation therapy sequelae, trauma, degenerative changes, infections, spondyloarthritis and osteonecrosis (6-10).

In this review, the MRI appearance of normal BM changes related to physiologic states, as well as the imaging features of benign and malignant diseases, are presented.

Techniques

MRI is the most sensitive imaging modality to evaluate the BM, with the signal intensity depending on the relative amount of protein, water, fat, and cells within the marrow.

The routine spine MRI protocol consists of T1-weighted (T1w), T2-weighted (T2w) and STIR sequences.

Spin-Echo (SE) T1w is the most accurate sequence to evaluate the cellular content, because of the contrast with fat content in yellow marrow. Fat tissue has a short T1 relaxation time, leading to high signal intensity on T1w images. Therefore, the signal intensity of the marrow is dependent on the proportion of red and yellow marrow.

T2w images, especially using Fast SE techniques, show a decreased contrast of the spinal marrow, because water and fat are closer in signal intensity.

Fat tissue signal suppression can be obtained both with fat saturation (SPIR or SPAIR, if a frequency-selective saturation radio-frequency pulse with the same resonance frequency as that of lipids is applied) or using STIR sequences (choosing an inversion time adequate to null the signal generated by fat) (11-15).

The latter approach has several practical advantages, including acquisition of more slices per unit of time, but reduced tissue specificity (16-20).

Hematopoietic marrow shows intermediate signal on STIR sequences, similar to that of muscle, whereas fatty marrow shows lower signal intensity than that of muscle.

Gadolinium-enhanced T1w images may be helpful in the assessment of neoplastic infiltration and evaluation of the extent of extramedullary spread as well as in the evaluation of infective/inflammatory pathology. However, as most bone diseases show hypointense signal on unenhanced T1-w sequences, enhancing lesions may be difficult to recognize when they become isointense to normal BM. For this reason, the post-contrast evaluation of the spine is mandatorily performed using T1w sequences with fat-suppression.

Nonroutine MRI sequences include diffusion-weighted imaging (DWI), MR spectroscopy (MRS), in- and out-of-phase MRI, and dynamic contrast-enhanced MRI (perfusion imaging).

DWI enables to measure the random motion of free water protons on a molecular basis by using different imaging sequences including steady-state free precession imaging, navigated SE DWI, and single-shot echo planar imaging (21-25).

In the last years, DWI has shown great potential for the differentiation of acute osteoporotic from neoplastic vertebral fractures. As far as DWI is concerned, it is hypothesized that edema formation in benign osteoporotic fractures results in increased diffusivity, while the cellular structure associated with neoplastic tissue acts to restrict water mobility, thereby decreasing diffusivity (26-30).

However, the usefulness of DWI in differentiating benign from metastatic spinal fractures is controversial. Due to both the spongy microstructure of the trabecular bone and the proximity of the lungs, soft tissue, or large vessels, substantial magnetic susceptibility variations occur, which severely reduce the magnetic field homogeneity as well as the transverse relaxation time $T2^*$, and thus complicate the MRI appearance, in particular with echo-planar imaging techniques. Numerous studies demonstrate significantly increased diffusivity with greater ADC values (typically between 1.2 and 2.0 $\times$ 10^{-3} mm^2/s) in osteoporotic fractures compared to malignant fractures or lesions (typically 0.7-1.3 $\times$ 10^{-3} mm^2/s). Moreover, several studies used the qualitative image contrast of diffusion-weighted acquisitions for differentiation of lesion etiology: a reliable lesion differentiation can be achieved particularly with diffusion-weighted steady-state free precession sequences, which depict malignant lesions as hyperintense relative to normal-appearing vertebral BM, in contrast to hypointense or isointense osteoporotic lesions (31-35).

MRS allows a noninvasive quantitative assessment of bone constituents, particularly fat, at the molecular level. A single or multi-voxel method can be used to assess one or more vertebral bodies and their fat content, which is related to weakened bone (36-

40), tipically expressed as a percentage (due to multiple lipid peaks) not as an absolute value (41-45).

Previous reports emphasized age- and sex- related physiologic changes of the fat content of the spinal BM (46-50). However, MRS is not widely used clinically as similar information can be achieved by a less expensive dual-energy x-ray absorptiometry (51-55).

Chemical-shift or opposed phase imaging relies on the fact that water and fat have different resonance frequencies. Indeed water and fat protons are in phase with one another at a TE of 4.6 milliseconds and 180° opposed at a TE of 2.4 milliseconds at 1.5 T. A given voxel containing both fat and water shows some signal intensity loss on out-phase images, while metastatic and infiltrative marrow neoplasms will destroy normal marrow and retain high water content with resultant high signal on out-phase imaging. This has proved beneficial in differentiating neoplastic and osteoporotic fractures (7, 56-60).

Also, dynamic contrast-enhanced MRI of BM has been used in patients with lymphoproliferative disease and diffuse marrow infiltration as well as in the assessment of response to chemotherapy. During Gadolinium-based contrast agent rapid intravenous administration, changes in longitudinal relaxation of vertebral marrow are measured and signal-time-intensity curves are reproduced. Various parameters have been used, such as maximum intensity, slope of the curve and contrast wash-out. BM perfusion decreases markedly with increasing age and in subjects with osteoporosis (61-65). In patients with marrow infiltration by focal or diffuse hematological malignancies, perfusion imaging shows higher peak enhancement percentage, enhancement slope and time to peak (63, 66-70)

Normal age-related bone marrow appearance and normal variants

Normal BM is composed of an intermixture of red (or hematopoietic) marrow, yellow (or fatty) marrow, and trabecular bone in varying proportions, based on the patient age and other factors.

Yellow marrow appears hyperintense on T1w images, because it is composed of fatty elements, and shows intermediate and high signal intensity on T2w SE and T2w fast Spin-Echo sequences, respectively. It saturates similarly to subcutaneous fat on T2w sequences with fat saturation and on STIR sequences (52, 57, 71-75).

Red marrow demonstrates low/intermediate signal intensity on T1w sequences compared to the disk, and shows intermediate signal intensity on T2w sequences, which can result in some difficulty in distinguishing red marrow from yellow marrow; it displays mild high signal intensity on STIR images.

Age profoundly affects vertebral marrow signal intensity and homogeneity at MR imaging (7, 52, 76-80).

The proportion of marrow fat cells normally increases in a diffuse and homogeneous manner with ageing, a process called fatty marrow "conversion" of red marrow, resulting in a progressive increase in marrow signal intensity on T1w images. BM conversion begins with long bones (from diaphysis and epiphysis to metaphysis) and then extends to the axial skeleton.

Marrow appearance shows a limited variation among vertebral bodies of the same person, as opposed to marked variability in different people of similar age and demographics.

The sacro-coccygeal region is the exception to this rule, where partial or diffuse fatty infiltration is commonly seen (12, 60, 81-84).

Four patterns of physiologic conversion of active hematopoietic red marrow to fatty BM in the vertebral bodies have been described on T1w SE images (Fig. 1) (85). In *pattern 1*, linear areas of high signal intensity parallel the basivertebral vein. The remainder of the vertebral body is uniformly low in signal intensity (red marrow). This pattern was observed in nearly one half of those younger than 20, and in essentially no one older than 30. In *pattern 2*, the conversion to fatty marrow is located at the periphery of the vertebral body, along the corners of the vertebral bodies and near the endplates, where bandlike and triangular regions of high signal intensity are found. In *pattern 3*, diffusely distributed areas of high signal intensity are seen and further subclassified based on their size: pattern 3a consists of numerous, indistinct, high signal intensity foci, measuring a few millimeters or less; pattern 3b consists of fairly well-marginated regions of high signal intensity, ranging in size from 0.5 to 1.5 cm. Approximately 85% of individuals older than 40

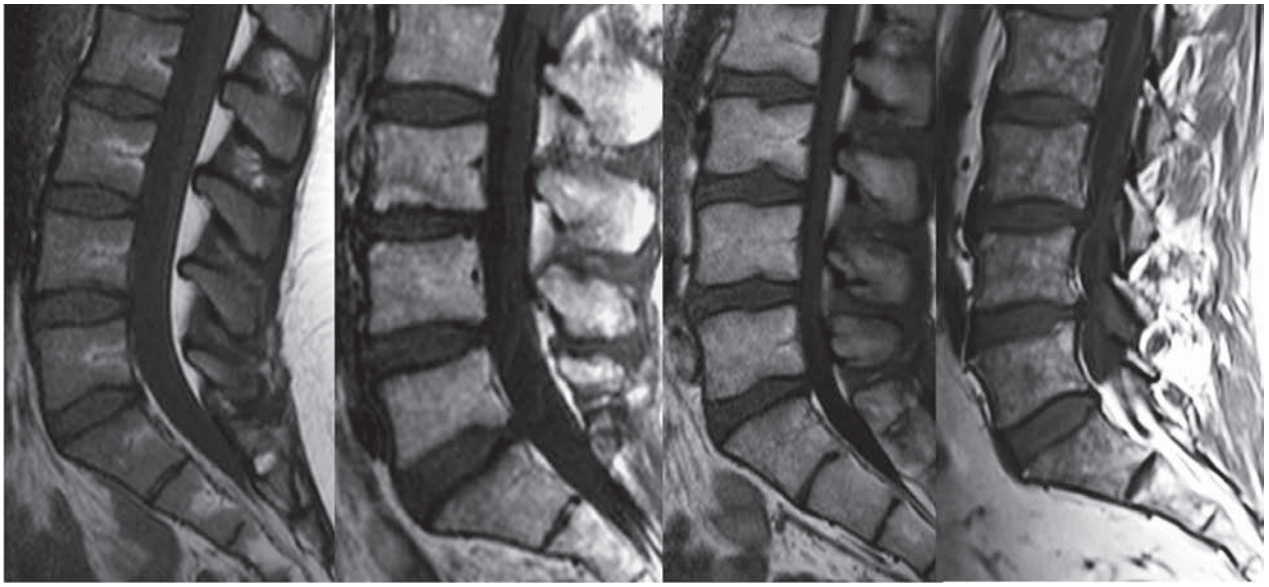

Figure 1. TSE T1w images on the sagittal plane. Patterns of physiologic conversion of active hematopoietic red marrow to fatty bone marrow: pattern 1 (A), 2 (B), 3a (C), 3b (D)

years show pattern 2, and approximately 75% show pattern 3.

Under normal circumstances, the vertebral BM is not composed entirely of either all red or all yellow marrow, but is intermixed, so accounting for its appearance on MR imaging. Marrow reconversion (from yellow to red BM) is a process that occurs during times of stress, in which the body requires increased blood cell production, such as in response to anemia or haematologic malignancies (Figure 2). It occurs in the reverse order of maturation and favors areas of residual hematopoietic sites (starting from the vertebral endplates). Thus, the finding of a diffuse T1w hypointensity of the vertebral bodies (usually more hypointense than the intervening disks) should always prompt a dosage of haemoglobin and circulating blood cells, as well as a serum protein electrophoresis analysis.

Normal variants and common findings

Diffuse heterogeneous patterns of spinal BM are relatively frequent findings, especially in subjects after the fourth decade of life. Usually they are related to a dissemination of foci of high signal intensity (fat nodules, Fig. 3); consequently, the adjacent normal red marrow appears with concave margins. This pattern, considered a non-significant finding, must be distinguished from the heterogeneous pattern related to the presence cellular marrow nodules, that may remain undistinguishable from significant marrow lesions; in this case, red marrow appears with convex margins on T1w sequences. Sometimes, red marrow islands appear as

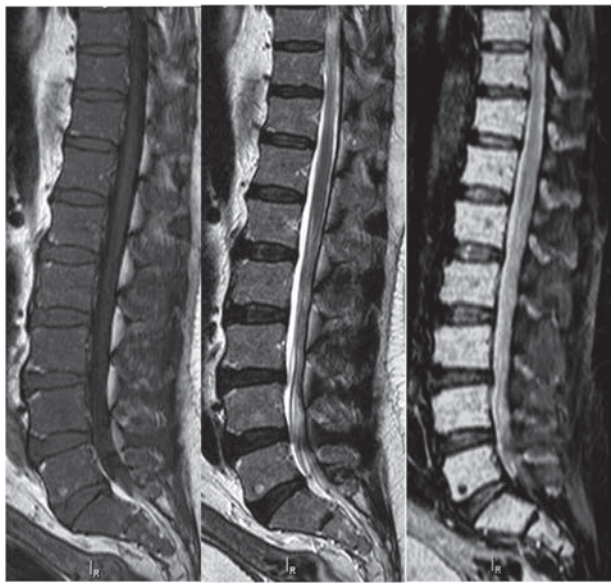

Figure 2. Multiple myeloma, diffuse pattern. TSE T1w (A), TSE T2w (B) and STIR (C) images on the sagittal plane

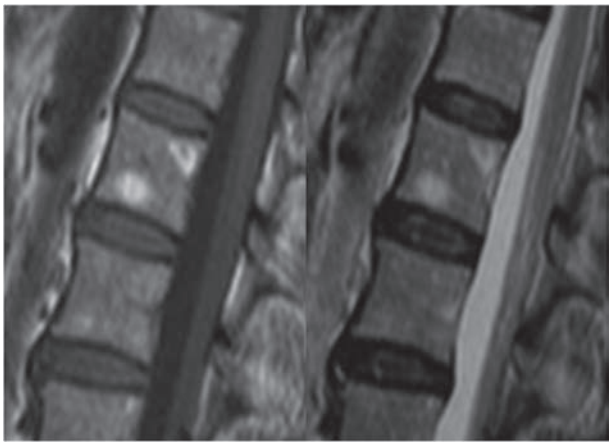

Figure 3. Fat marrow nodules. TSE T1w (A) and TSE T2w (B) images

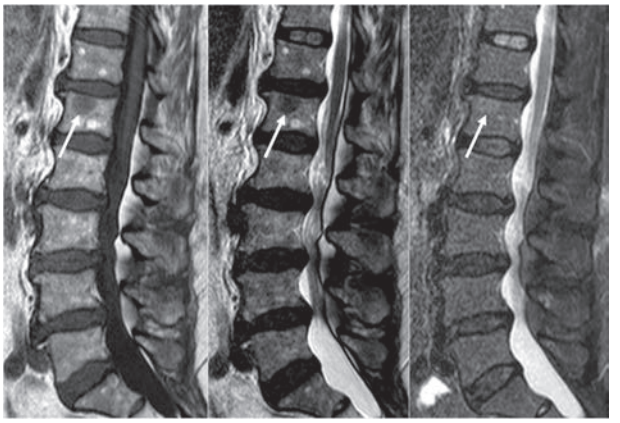

Figure 4. Cellular marrow nodule (arrows). TSE T1w (A), TSE T2w (B) and STIR (C) images

small hypointense spots within a fat marrow nodule (*bull's eye* sign).

Focal normal variants as large nodules of fatty marrow or hypercellular red marrow (Fig. 4) can be occasionally observed on T1w sequences, more often in elderly patients.

Red flags that must be considered in the evaluation of these signal abnormalities include: marked hypointensity, homogeneous low signal intensity on T1w sequence with sharp margins, increase in size/number on follow-up MR and any change in trabecular or cortical bone on Computed Tomography (CT).

Other very frequently observed changes in BM signal are represented by benign vertebral lesions, in particular hemangiomas, enostosis (compact bone island) and, less frequently, benign notochordal cells tumors.

Vertebral hemangioma (VH) is the most common benign vertebral tumor and it is usually an incidental finding. It consists of vascular and fatty stroma with sparse thick trabeculae. On MRI, VH typically presents as a roundish T1w/T2w hyperintense lesions with variable fat suppression (depending on the amount of fat components) and intense contrast-enhancement. They can be multiple and are located in the soma or, less frequently, in the posterior arch. The presence of thickened trabeculae within the lesion is helpful to distinguish hemangioma from fat marrow nodules (Fig. 5). Aggressive hemangiomas may show

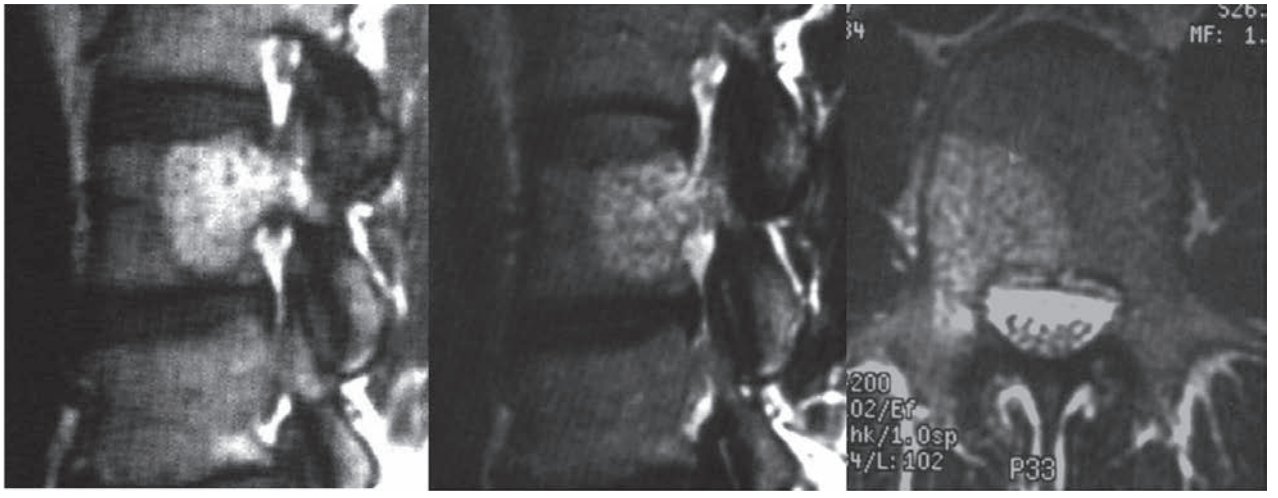

Figure 5. Vertebral hemangioma. TSE T1w (A), TSE T2w (B) images on the sagittal plane and TSE T2w image on the axial plane (C)

intermediate/low signal on T1w sequence, involvement of the entire vertebral body with extension to neural arch, cortical expansion, irregular honeycombing, and soft-tissue mass and avid enhancement. In case of doubts a CT scan may be helpful demonstrating the typical "palisading" appearance; angiography reveals the vascularity and arterial embolization may be helpful (55, 62, 86-90).

Enostosis is considered a developmental hamartomatous lesion consisting of lamellar compact bone in the spongious bone. It shows low signal on all MR sequences, without enhancement after gadolinium administration.

Enostosis, especially in the lumbosacral region, should be distinguished from the less common benign notochordal cell tumors (BNCT), which are increasingly accepted as intraosseous benign lesions of notochordal cell origin. These lesions may be safely followed without evidence of malignant transformation, which emphasizes the importance of distinction of BNCTs from chordomas (91).

BNCTs are usually intraosseous, whereas >90% of chordomas are both intra- and extra-osseous; moreover, they show mild osteosclerosis, without bone destruction, whereas all chordomas show variable osteolysis; finally, BNCTs do not enhance, whereas chordomas do, although with variable intensity(92).

Anemias and bone marrow insufficiency

Anemia, the most common disorder of the blood, is characterized by a diminished quantity of hemoglobin and can be caused by various etiologies. A decrease in hemoglobin due to iron- or vitamin-deficiency stimulates an overall increase in the amount of hematopoietic marrow, which, however, can also be seen in smokers, obese individuals, and marathon runners.

Red marrow hypertrophy appears on MRI as diffuse hypointensity on T1w images, with a corresponding hyperintense signal on T2w and STIR sequences and a typical mild diffuse enhancement of red marrow after administration of gadolinium-based contrast agents.

In patients with severe thalassemia it is not unusual to find areas of extramedullary hematopoiesis, particularly in the paravertebral soft tissues, appearing as soft-tissue masses sometimes even mimicking tumors (Fig. 6).

MRI can also show BM hypointensity on T2w images related to iron deposition in patients who received multiple blood transfusions.

Conversely, BM insufficiency (i.e. aplastic anemia) is characterized by an increase of fat, resulting in high signal on T1w sequences, and low signal on STIR images (93).

Figure 6. TSE T2w image on the coronal plane (A); axial balanced-GrE image on the axial plane (B). Areas of extramedullary hematopoiesis appearing as soft-tissue masses in a patient with severe thalassemia.

Osteonecrosis

Kummel's disease (post-traumatic vertebral osteonecrosis or avascular necrosis) represents a failure of the fracture healing process, with the development of an avascular zone below the superior endplate (94, 95) resulting in an osteonecrotic cavity, usually after weeks or months from trauma or osteoporotic fracture.

Gas or fluid can migrate from the adjacent degenerated disk into this cavity giving a "vacuum cleft" or "fluid" sign, respectively. The former appears as a black line below the upper endplate on both CT and all MRI sequences, while the latter is characterized by water density at CT and high signal intensity on STIR and T2w images.

Both these signs stand against infection or neoplasm(96). Particularly, the presence of gas in a collapsed vertebral body is diagnostic of Kummel's disease (97).

Osteonecrosis may cause insufficiency fractures with end-plate compressions by the adjacent intervertebral disks leading to the characteristic biconcave deformity (98).

Infective-inflammatory disease

Infections of the spine include spondylitis (infection of the bone and BM, i.e. ostemyelitis), discitis, spondylodiscitis and spondylarthritis (septic arthritis of the facet joints).

Pyogenic spondylitis, most often caused by Staphylococcus aureus, has a predilection for the lumbar region. In most cases, two adjacent vertebral bodies and the intervening disk are infected. Imaging patterns indicative of infection include decreased BM signal on T1w images, and increased signal on T2w and STIR images in the vertebral body adjacent to the involved disk space, disk hyperintensity on T2w images with intense and homogeneous enhancement after contrast injection, and, sometimes, paraspinal inflammatory tissue or fluid collection (99-101).

Unlike pyogenic infections, spinal tuberculosis is thought to originate in the vertebral body and spread beneath the longitudinal ligaments to involve adjacent vertebral bodies, sparing the disk, possibly because Mycobacterium Tuberculosis does not produce proteolytic enzymes. In addition to the disk preservation, other characteristics of tuberculosis include skip lesions and involvement of multiple vertebral bodies or only a portion of a vertebral body (such as the posterior elements). Paraspinal fluid collections are also common (6).

Non-infective inflammatory disease: degenerative

Modic provided a formal classification of vertebral endplate and subchondral BM degenerative changes based on a study of 474 patients, most of them with chronic low back pain (102). In advanced cases, these changes may involve a large part of the vertebral body, but they are always centered on the intersomatic disk space.

Type 1 changes are hypointense on T1w and hyperintense on T2w images, due to BM edema and inflammation. Type 2 changes appear hyperintense on T1w and isointense or slightly hyperintense on T2w images, and are associated with the conversion of hemopoietic BM into fatty marrow as a result of marrow ischemia. Modic type 3 changes are hypointense on both T1w and T2w sequences and are thought to represent subchondral bone sclerosis.

Mixed-type 1-2 and 2-3 Modic changes have also been reported, suggesting that these changes can convert from one type to another and that they represent different stages of the same pathologic process (103).

Non-infective inflammatory disease: spondyloarthritis

Seronegative spondyloarthropathies are inflammatory diseases that affect the axial skeleton, particularly the sacroiliac joints. These entities include ankylosing spondylitis, psoriatic arthritis, reactive arthritis, and arthritis associated with inflammatory bowel disease.

Spinal changes associated with spondyloarthritis include florid anterior spondylitis (*Romanus lesion*, i.e. reduced signal intensity of the anterior and posterior edges of the vertebral endplates on T1w images and increased signal intensity on STIR images, representing BM edema or osteitis), florid diskitis (*Andersson lesion*, disk-centered abnormalities of one or both con-

tiguous vertebrae, appearing hypointense on T1w- and hyperintense on STIR images), ankylosis, insufficiency fractures of the ankylosed spine, syndesmophytes, arthritis of the apophyseal and costo-vertebral joints and enthesitis of the interspinal ligaments. These lesions are not pathognomonic for ankylosing spondylitis because they can also be seen in other spondyloarthropathies (104).

SAPHO syndrome (synovitis, acne, pustulosis, hyperostosis and osteitis) should be included in the differential diagnosis in a patient with a "curvilinear" or "semicircular" pattern of signal abnormalities of contiguous vertebral body (63, 105-108).

Non-infective inflammatory disease: chronic recurrent multifocal osteomyelitis

Chronic recurrent multifocal osteomyelitis (CRMO) is an uncommon auto-inflammatory disease mostly affecting children and adolescents, presenting with multifocal bone pain secondary to sterile osseous inflammation. It is characterized by a relapsing-remitting course. The long bones of the lower extremities and sterno-clavear joint are more frequently affected with possible spine involvement. Imaging studies are important for the diagnosis and detection of asymptomatic lesions.

STIR sequences are useful to depict foci of BM edema (Fig. 7) and to assess the treatment response (109). Bone biopsy may be necessary to exclude other diseases, including malignancy and infections.

Non-infective inflammatory disease: Paget's disease

Paget's disease is a chronic metabolically active bone disease, characterized by a disturbance in bone modelling and remodelling due to an increase in osteoblastic and osteoclastic activity.

The spine is the second most commonly affected site (53%), after the pelvis (70%).

Paget's disease is primarily a disorder of bone, and BM is only secondarily involved. The mixed hypervascular phase is characterized by the presence of areas of vertebral low signal on T1w images and mild high signal on T2w images. In the sclerotic phase a low signal on both T1w and T2w images in the vertebra is due to increased trabecular thickness, sclerosis and marrow fibrosis. In the advanced stages, the fatty transformation leads to high signal on both T1w and T2w images (110).

Figure 7. Chronic recurrent multifocal osteomyelitis. TSE T1w (A), TSE T2w (B) and STIR (C) images

Traumatic bone marrow edema

MRI is nowaydays recognized as the most sensitive technique (even more than CT) to evaluate minor vertebral trauma, due to its unsurpassed sensitivity to detect BM edema, even without evidence of fracture deformity or cortical failure (111).

Indeed, MRI with STIR sequences are the necessary diagnostic pre-requisite (together with the clinical evaluation) for selecting patients amenable to percutaneous interventional procedures such as vertebroplasty and kiphoplasty.

Aside from its role in obvious post-traumatic fractures, MRI is very useful in the differentiation between benign and malignant vertebral fractures, a common clinical problem, as they both typically occurr in the elderly population without adequate trauma.

Features suggestive of metastatic compression fractures include the presence of a convex posterior border of the vertebral body, abnormal signal intensity of the pedicle or posterior element, an epidural mass, a focal paraspinal mass and other spinal metastases. Conversely, a low-signal-intensity band on T1w and T2w

images (corresponding to the fracture line or trabecular impaction), spared normal BM signal intensity of the vertebral body, retropulsion of a posterior bone fragment and multiple compression fractures are suggestive of acute osteoporotic compression fractures (112).

However, conventional MRI is not always specific in the differentiation of acute osteoporotic and malignant vertebral fractures. In this context DWI may be useful: malignant fractures show ADC values ranging from 0.7 to 1.0 x 10^{-3} mm^2/s, while osteoporotic or traumatic fractures show ADC values from 1.0 to 2.0 x 10^{-3} mm^2/s(113). Unfortunately, all published studies show a remarkable overlap, thus limiting the value of quantitative DWI in differentiating between benign and malignant fractures.

Bone metastasis

Metastases are the most common malignant tumors affecting the skeletal system.

Spine is a frequent target of metastatic spread from various primary tumors such as breast, lung and prostate carcinomas. MRI is the most sensitive technique for the detection of BM metastasis, even if trabecular or cortical bone is not destroyed (unlike bone scintigraphy). Whole-body MRI, possibly with diffusion-weighted whole-body imaging with background body signal suppression (DWIBS) sequences, represents a promising technique for tumor staging which allows for assessment of the whole skeletal system, with a higher sensitivity than PET-CT(114, 115).

The combination of unenhanced T1w and STIR sequences allows the detection of BM abnormalities (116, 117). On T1w images, metastatic lesions are identified by the replacement of normal fat marrow, resulting in a focal or diffuse hypointense signal. On T2w and STIR sequence neoplastic lesions appear hyperintense due to increased content of water within the metastatic lesions; blastic metastasis may present low signal intensity on T2w and STIR images, depending on the degree of sclerosis. In this case, evaluation of the margins may be helpful to differentiate blastic metastasis (with irregular shape) from enostosis (more regular).

In case of suspected extension into the surrounding tissues (paravertebral or epidural space) additional sequences, such as T2w and contrast-enhanced fat-saturated T1w sequences in the axial and coronal planes may be useful to better delineate the lesion (118).

Multiple myeloma and leukemia

Multiple myeloma is characterized by a multifocal malignant proliferation of monoclonal plasma cells within the BM. The spine is the most commonly involved site.

MRI may be normal or may show different patterns of BM involvement, focal (plasmocytoma), diffuse or micronodular. Lesions are characterized by low signal intensity on T1w images, hyperintensity on STIR sequence, with post-gadolinium enhancement and high perfusion values on DCE-PWI (119-121). Furthermore, MRI can demonstrate concurrent pathologic fractures that can mimic a benign pattern.

Leukemia may present with similar findings and may be difficult to distinguish it from diffuse myeloma on the basis of MRI findings alone (119, 122).

Myelofibrosis

Primary myelofibrosis is a chronic myeloproliferative disorder resulting in BM fibrosis.

On MRI, it appears as diffuse low signal intensity of the BM on all sequences, due to the increase in marrow cells and reduction in fat cells in the early stages, or due to extensive marrow fibrosis in the late stages.

Extramedullary hematopoiesis, with paravertebral soft tissue masses and hepatosplenomegaly, may be found in the most advanced stages of the disease.

Lymphoma

BM lymphoma can occasionally present as primary extranodal disease, although it is more frequently due to a secondary involvement from disseminated disease.

BM involvement is more frequently seen in patients with non-Hodgkin's lymphoma, while it is unusual in patients with Hodgkin's lymphoma (only 4-14% of cases) (123).

On MRI, lymphomatous lesions, which can be focal or multiple/diffuse, show T1 hypointense signal

with variable T2 signal intensity, sometimes hypointense because of their high cellularity. Lymphoma typically permeates through the cortex and into surrounding soft tissues (including the epidural space) without causing cortical destruction.

Bone marrow necrosis and non-traumatic avascular necrosis

BM necrosis is a rare hematologic disorder in which a microvascular insult leads to necrosis of myeloid tissue and medullary stroma with preservation of cortical bone and spicular architecture (124-127).

On MRI, it is characterized by diffuse involvement of BM within the posterior aspect of vertebral bodies with a "geographic" pattern of signal abnormalities. The lesions show central hyperintensity on T1-w and T2-w images surrounded by a peripheral band of hypointense signal that enhances after contrast administration (Fig. 8) (128-130).

Non-traumatic avascular necrosis shares several imaging features with BM necrosis. In contrast to the strong association of BM necrosis with malignancy, avascular necrosis does not imply any prognostic significance. It is typically associated with corticosteroids, ethanol abuse and hemoglobinopathies (131-134).

Lesions may display T1w and T2w imaging findings similar to those of BM necrosis, but a progression to vertebral body collapse is often observed. Definitive diagnosis requires BM biopsy with histological examination in which avascular necrosis is typified by loss of normal spicular architectural.

Treatment response assessment

Radiation therapy induces characteristic time-dependent changes in BM, as in other tissues (135). Early post-radiation changes (first week) are characterized by diffuse hyperintensity on STIR images without significant signal changes on T1w images. With time, BM edema subsides; in this phase, early fatty infiltration and fibrosis are characterized by heterogeneous T1w hyperintensity. Finally, with fatty conversion (which is not necessarily permanent), the MRI signal evolves into homogeneous and diffusely hyperintense T1 signal with corresponding hypointense STIR signal.

Three histologic stages of BM remodeling can be defined after the initiation of chemotherapy. During the first week, increased permeability and dilatation of the BM sinuses causes acute edema, corresponding to a decrease in T1w signal intensity. The second stage of BM remodeling occurs as early as the second week after chemotherapy initiation. Histologically,

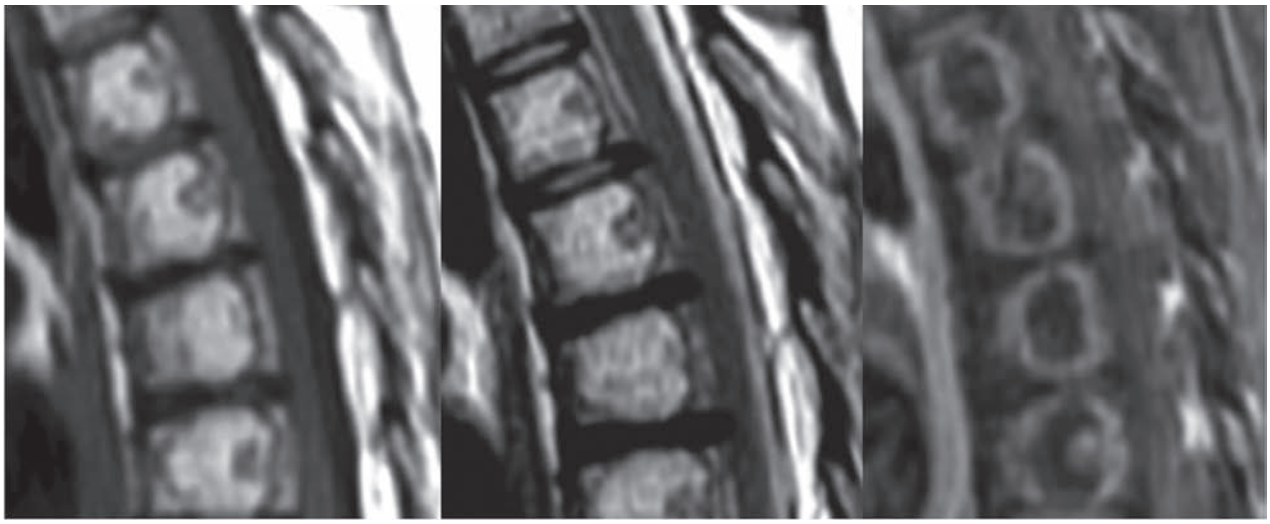

Figure 8. Bone marrow avascular necrosis. TSE T1w (A), TSE T2w (B) and post-contrast injection fat-suppressed TSE T1w (C) images.

there is decreased marrow cellularity, as well as early fatty conversion to multilocular adipocytes. On MR imaging, these pathologic changes cause an increased T1w signal and decreased intensity on fluid-sensitive sequences. Finally, with the completion of chemotherapy, multilocular adipocytes are replaced by unilocular fat cells. These unilocular adipocytes and stromal cells form multifocal aggregates and are thought to be necessary for the regeneration of normal hematopoietic tissue. Early reconversion on MR imaging is seen as diffuse hematopoietic foci of T1 hypointensity and modest hyperintensity on fluid-sensitive sequences, and they must be differentiated from relapse; in these cases, contrast administration may be useful.

Furthermore, the reconversion process may be enhanced by administration of granulocyte colony-stimulating factor (GCSF), which activates the hematopoietic marrow and decreases the period of aplasia after chemotherapy. The differentiation between this reconverted, highly cellular normal hematopoietic marrow and a recurrent tumor after chemotherapy is not possible with conventional MR techniques (136).

The response of focal marrow lesions to therapy may be characterized, along with their reduction in size, by the appearance of a peripheral halo of fatty marrow, with characteristic high signal intensity on T1-weighted images. Contrasting with this "fatty" halo, a "cellular" halo may be observed at the periphery of neoplastic lesions, consisting in a faint border with a low signal on T1 and high signal intensity on STIR/T2 fat suppressed images, which is interpreted as indicative of an "active" or "aggressive" tumoral lesion. In/out phase imaging can be useful in pointing out these findings.

Conclusions

MRI is the most sensitive technique for assessing BM signal abnormalities. Knowledge of normal age-related BM appearance, normal variants and patterns of involvement in focal and diffuse bone diseases (Tab. 1) is essential, together with clinical and laboratory data, to narrow the list of the possible differential diagnoses. The radiologist should be familiar with these signal changes, as they can sometimes be discovered incidentally. In this context, it is equally important not to attribute pathological significance to benign alterations and to promptly detect signs of malignant diseases (137).

Table 1. Differential diagnosis of abnormal marrow signal within the spinal bone marrow on T1w- imaging [57].

Focal T1 signal increase	Diffuse/multifocal T1 signal increase	Focal T1 signal decrease	Diffuse/multifocal T1 signal decrease
focal fatty marrow	radiation treatment	**endplate centered:** degenerative endplate changes, osteomyelitis, amyloid	hematopoietic hyperplasia
solitary hemangioma	osteoporosis	**Primarily in vertebral body:** atypical hemangioma, fracture, malignancy, fibrous dysplasia, metastasis, myeloma, lymphoma	neoplasm
degenerative disk disease	multiple hemangiomas	**Posterior element centered:** primary bone tumor, fracture	renal osteodystrophy
Paget's disease	melanoma metastasis		sarcoidosis
BM hemorrhage	myeloma		spondyloarthropathy
lipoma	lymphoma		myelofibrosis mastocytosis hemosiderosis Gaucher's disease gout

References

1. Hays K. Physiology of normal bone marrow. Semin Oncol Nurs 1990; 6(1): 3-8.
2. Di Zazzo E, Porcile C, Bartollino S, Moncharmont B. Critical Function of PRDM2 in the Neoplastic Growth of Testicular Germ Cell Tumors. Biology (Basel) 2016; 5(4).
3. Dragoni S, Turin I, Laforenza U, Potenza DM, Bottino C, Glasnov TN, et al. Store-operated Ca2+ entry does not control proliferation in primary cultures of human metastatic renal cellular carcinoma. Biomed Res Int 2014; 2014: 739494.
4. Potenza DM, Guerra G, Avanzato D, Poletto V, Pareek S, Guido D, et al. Hydrogen sulphide triggers VEGF-induced intracellular Ca(2)(+) signals in human endothelial cells but not in their immature progenitors. Cell Calcium 2014; 56(3): 225-34.
5. Nurzynska D, Di Meglio F, Castaldo C, Latino F, Romano V, Miraglia R, et al. Flatfoot in children: anatomy of decision making. Ital J Anat Embryol 2012; 117(2): 98-106.
6. Long SS, Yablon CM, Eisenberg RL. Bone marrow signal alteration in the spine and sacrum. AJR Am J Roentgenol 2010; 195(3): W178-200.
7. Reginelli A, Zappia M, Barile A, Brunese L. Strategies of imaging after orthopedic surgery. Musculoskeletal Surg 2017; 101.
8. Splendiani A, Bruno F, Patriarca L, Barile A, Di Cesare E, Masciocchi C, et al. Thoracic spine trauma: advanced imaging modality. Radiol Med 2016; 121(10): 780-92.
9. Splendiani A, Perri M, Grattacaso G, Di Tunno V, Marsecano C, Panebianco L, et al. Magnetic resonance imaging (MRI) of the lumbar spine with dedicated G-scan machine in the upright position: a retrospective study and our experience in 10 years with 4305 patients. Radiol Med 2016; 121(1): 38-44.
10. Ripani M, Continenza MA, Cacchio A, Barile A, Parisi A, De Paulis F. The ischiatic region: normal and MRI anatomy. J Sports Med Phys Fitness 2006; 46(3): 468-75.
11. Shah LM, Hanrahan CJ. MRI of spinal bone marrow: part I, techniques and normal age-related appearances. AJR Am J Roentgenol 2011; 197(6): 1298-308.
12. Barile A, Arrigoni F, Bruno F, Guglielmi G, Zappia M, Reginelli A, et al. Computed Tomography and MR Imaging in Rheumatoid Arthritis. Radiol Clin North Am 2017.
13. Di Pietto F, Chianca V, de Ritis R, Cesarano E, Reginelli A, Barile A, et al. Postoperative imaging in arthroscopic hip surgery. Musculoskeletal Surg 2017; 101: 43-9.
14. Masciocchi C, Conchiglia A, Conti L, Barile A. Imaging of insufficiency fractures. Geriatric Imaging: Springer-Verlag Berlin Heidelberg; 2013. p. 83-91.
15. Masciocchi C, Lanni G, Conti L, Conchiglia A, Fascetti E, Flamini S, et al. Soft-tissue inflammatory myofibroblastic tumors (IMTs) of the limbs: Potential and limits of diagnostic imaging. Skelet Radiol 2012; 41(6): 643-9.
16. Mirowitz SA, Apicella P, Reinus WR, Hammerman AM. MR imaging of bone marrow lesions: relative conspicuousness on T1-weighted, fat-suppressed T2-weighted, and STIR images. AJR Am J Roentgenol 1994; 162(1): 215-21.
17. Masciocchi C, Conti L, D'Orazio F, Conchiglia A, Lanni G, Barile A. Errors in musculoskeletal MRI. Errors in Radiology: Springer-Verlag Milan; 2012. p. 209-17.
18. Barile A, Regis G, Masi R, Maggiori M, Gallo A, Faletti C, et al. Musculoskeletal tumours: Preliminary experience with perfusion MRI. Radiol Med 2007; 112(4): 550-61.
19. Splendiani A, Perri M, Marsecano C, Vellucci V, Michelini G, Barile A, et al. Effects of serial macrocyclic-based contrast materials gadoterate meglumine and gadobutrol administrations on gadolinium-related dentate nuclei signal increases in unenhanced T1-weighted brain: a retrospective study in 158 multiple sclerosis (MS) patients. Radiol Med 2017.
20. Bruno F, Smaldone F, Varrassi M, Arrigoni F, Barile A, Di Cesare E, et al. MRI findings in lumbar spine following O2-O3 chemiodiscolysis: A long-term follow-up. Interv Neuroradiol 2017; 23(4): 444-50.
21. Baur A, Stabler A, Huber A, Reiser M. Diffusion-weighted magnetic resonance imaging of spinal bone marrow. Semin Musculoskelet Radiol 2001; 5(1): 35-42.
22. Arrigoni F, Barile A, Zugaro L, Splendiani A, Di Cesare E, Caranci F, et al. Intra-articular benign bone lesions treated with Magnetic Resonance-guided Focused Ultrasound (MRgFUS): imaging follow-up and clinical results. Med Oncol 2017; 34(4).
23. Giordano AV, Arrigoni F, Bruno F, Carducci S, Varrassi M, Zugaro L, et al. Interventional Radiology Management of a Ruptured Lumbar Artery Pseudoaneurysm after Cryoablation and Vertebroplasty of a Lumbar Metastasis. Cardiovasc Intervent Radiol 2017; 40(5): 776-9.
24. Barile A, Arrigoni F, Zugaro L, Zappia M, Cazzato RL, Garnon J, et al. Minimally invasive treatments of painful bone lesions: state of the art. Med Oncol 2017; 34(4).
25. Splendiani A, D'Orazio F, Patriarca L, Arrigoni F, Caranci F, Fonio P, et al. Imaging of post-operative spine in intervertebral disc pathology. Musculoskeletal Surg 2017; 101: 75-84.
26. Raya JG, Dietrich O, Reiser MF, Baur-Melnyk A. Methods and applications of diffusion imaging of vertebral bone marrow. J Magn Reson Imaging 2006; 24(6): 1207-20.
27. Cazzato RL, Garnon J, Ramamurthy N, Koch G, Tsoumakidou G, Caudrelier J, et al. Percutaneous image-guided cryoablation: current applications and results in the oncologic field. Med Oncol 2016; 33(12).
28. Masciocchi C, Zugaro L, Arrigoni F, Gravina GL, Mariani S, La Marra A, et al. Radiofrequency ablation versus magnetic resonance guided focused ultrasound surgery for minimally invasive treatment of osteoid osteoma: a propensity score matching study. Eur Radiol 2016; 26(8): 2472-81.
29. Masciocchi C, Arrigoni F, Marra AL, Mariani S, Zugaro L, Barile A. Treatment of focal benign lesions of the bone: MRgFUS and RFA. Br J Radiol 2016; 89(1066).
30. Patriarca L, Letteriello M, Di Cesare E, Barile A, Gallucci M, Splendiani A. Does evaluator experience have an im-

pact on the diagnosis of lumbar spine instability in dynamic MRI? Interobserver agreement study. Neuroradiol J 2015; 28(3): 341-6.
31. Dietrich O, Geith T, Reiser MF, Baur-Melnyk A. Diffusion imaging of the vertebral bone marrow. NMR Biomed 2017; 30(3).
32. Zoccali C, Rossi B, Zoccali G, Barbarino E, Gregori L, Barile A, et al. A new technique for biopsy of soft tissue neoplasms: a preliminary experience using MRI to evaluate bleeding. Minerva Med 2015; 106(2): 117-20.
33. Arrigoni F, Gregori LM, Zugaro L, Barile A, Masciocchi C. MRgFUS in the treatment of MSK lesions: A review based on the experience of the university of L'aquila, Italy. Transl Cancer Res 2014; 3(5): 442-8.
34. Splendiani A, Ferrari F, Barile A, Masciocchi C, Gallucci M. Occult neural foraminal stenosis caused by association between disc degeneration and facet joint osteoarthritis: Demonstration with dedicated upright MRI system. Radiol Med 2014; 119(3): 164-74.
35. Masciocchi C, Conchiglia A, Gregori LM, Arrigoni F, Zugaro L, Barile A. Critical role of HIFU in musculoskeletal interventions. Radiol Med 2014; 119(7): 470-5.
36. Schellinger D, Lin CS, Hatipoglu HG, Fertikh D. Potential value of vertebral proton MR spectroscopy in determining bone weakness. AJNR Am J Neuroradiol 2001; 22(8): 1620-7.
37. Pierot L, Söderman M, Bendszus M, White P, Muto M, Turjman F, et al. Statement of ESMINT and ESNR regarding recent trials evaluating the endovascular treatment at the acute stage of ischemic stroke. Neuroradiology 2013; 55(11): 1313-8.
38. Izzo R, Guarnieri G, Guglielmi G, Muto M. Biomechanics of the spine. Part I: Spinal stability. Eur J Radiol 2013; 82(1): 118-26.
39. Masala S, Nano G, Marcia S, Muto M, Fucci FPM, Simonetti G. Osteoporotic vertebral compression fractures augmentation by injectable partly resorbable ceramic bone substitute (Cerament™|SPINE SUPPORT): A prospective nonrandomized study. Neuroradiology. 2012; 54(6): 589-96.
40. Guarnieri G, Vassallo P, Pezzullo MG, Laghi F, Zeccolini F, Ambrosanio G, et al. A comparison of minimally invasive techniques in percutaneous treatment of lumbar herniated discs a review. Neuroradiol J 2009; 22(1): 108-21.
41. Schwartz AV, Sigurdsson S, Hue TF, Lang TF, Harris TB, Rosen CJ, et al. Vertebral bone marrow fat associated with lower trabecular BMD and prevalent vertebral fracture in older adults. J Clin Endocrinol Metab 2013; 98(6): 2294-300.
42. Muto M, Perrotta V, Guarnieri G, Lavanga A, Vassallo P, Reginelli R, et al. Vertebroplasty and kyphoplasty: Friends or foes? Radiol Med 2008; 113(8): 1171-84.
43. Lanzillo R, Prinster A, Scarano V, Liuzzi R, Coppola G, Florio C, et al. Neuropsychological assessment, quantitative MRI and ApoE gene polymorphisms in a series of MS patients treated with IFN beta-1b. J Neurol Sci 2006; 245(1-2): 141-5.
44. Cappabianca S, Colella G, Russo A, Pezzullo M, Reginelli A, Iaselli F, et al. Maxillofacial fibrous dysplasia: personal experience with gadoliniumenhanced magnetic resonance imaging. Radiol Med 2008; 113(8): 1198-210.
45. Cappabianca S, Scuotto A, Iaselli F, Pignatelli di Spinazzola N, Urraro F, Sarti G, et al. Computed tomography and magnetic resonance angiography in the evaluation of aberrant origin of the external carotid artery branches. Surg Radiol Anat 2012; 34(5): 393-9.
46. Kugel H, Jung C, Schulte O, Heindel W. Age- and sex-specific differences in the 1H-spectrum of vertebral bone marrow. J Magn Reson Imaging 2001; 13(2): 263-8.
47. Iudici M, Cuomo G, Vettori S, Bocchino M, Sanduzzi Zamparelli A, Cappabianca S, et al. Low-dose pulse cyclophosphamide in interstitial lung disease associated with systemic sclerosis (SSc-ILD): efficacy of maintenance immunosuppression in responders and non-responders. Semin Arthritis Rheum 2015; 44(4): 437-44.
48. Valentini G, Marcoccia A, Cuomo G, Vettori S, Iudici M, Bondanini F, et al. Early systemic sclerosis: analysis of the disease course in patients with marker autoantibody and/or capillaroscopic positivity. Arthritis Care Res (Hoboken) 2014; 66(10): 1520-7.
49. Valentini G, Marcoccia A, Cuomo G, Vettori S, Iudici M, Bondanini F, et al. Early systemic sclerosis: marker autoantibodies and videocapillaroscopy patterns are each associated with distinct clinical, functional and cellular activation markers. Arthritis Res Ther 2013; 15(3): R63.
50. Mandato Y, Reginelli A, Galasso R, Iacobellis F, Berritto D, Cappabianca S. Errors in the radiological evaluation of the alimentary tract: part I. Semin Ultrasound CT MR 2012; 33(4): 300-7.
51. Nouh MR, Eid AF. Magnetic resonance imaging of the spinal marrow: Basic understanding of the normal marrow pattern and its variant. World J Radiol 2015; 7(12): 448-58.
52. Cappabianca S, Colella G, Pezzullo MG, Russo A, Iaselli F, Brunese L, et al. Lipomatous lesions of the head and neck region: Imaging findings in comparison with histological type. Radiol Med 2008; 113(5): 758-70.
53. Cappabianca S, Iaselli F, Reginelli A, D'Andrea A, Urraro F, Grassi R, et al. Value of diffusion-weighted magnetic resonance imaging in the characterization of complex adnexal masses. Tumori 2013; 99(2): 210-7.
54. Cappabianca S, Iaselli F, Negro A, Basile A, Reginelli A, Grassi R, et al. Magnetic resonance imaging in the evaluation of anatomical risk factors for pediatric obstructive sleep apnoea-hypopnoea: a pilot study. Int J Pediatr Otorhinolaryngol 2013; 77(1): 69-75.
55. Grassi R, Lombardi G, Reginelli A, Capasso F, Romano F, Floriani I, et al. Coccygeal movement: assessment with dynamic MRI. Eur J Radiol 2007; 61(3): 473-9.
56. Ragab Y, Emad Y, Gheita T, Mansour M, Abou-Zeid A, Ferrari S, et al. Differentiation of osteoporotic and neoplastic vertebral fractures by chemical shift {in-phase and out-of phase} MR imaging. Eur J Radiol 2009; 72(1): 125-33.
57. Zappia M, Cuomo G, Martino MT, Reginelli A, Brunese

L. The effect of foot position on Power Doppler Ultrasound grading of Achilles enthesitis. Rheumatol Int 2016; 36(6): 871-4.
58. Reginelli A, Russo A, Maresca D, Martiniello C, Cappabianca S, Brunese L. Imaging Assessment of Gunshot Wounds. Semin Ultrasound CT MRI 2015; 36(1): 57-66.
59. Briganti F, Tedeschi E, Leone G, Marseglia M, Cicala D, Giamundo M, et al. Endovascular treatment of vertebrovertebral arteriovenous fistula. A report of three cases and literature review. Neuroradiol J 2013; 26 (3): 339-346, 2013.
60. Pinto A, Pinto F, Faggian A, Rubino G, Caranci F, Macarini L, et al. Sources of error in emergency ultrasonography. Critical Ultrasound Journal 2013; 5 (suppl. 1): 1-5.
61. Griffith JF, Yeung DK, Antonio GE, Lee FK, Hong AW, Wong SY, et al. Vertebral bone mineral density, marrow perfusion, and fat content in healthy men and men with osteoporosis: dynamic contrast-enhanced MR imaging and MR spectroscopy. Radiology 2005; 236(3): 945-51.
62. Reginelli A, Silvestro G, Fontanella G, Sangiovanni A, Conte M, Nuzzo I, et al. Validation of DWI in assessment of radiotreated bone metastases in elderly patients. Int J Surg 2016; 33 Suppl 1: S148-53.
63. Perrotta FM, Astorri D, Zappia M, Reginelli A, Brunese L, Lubrano E. An ultrasonographic study of enthesis in early psoriatic arthritis patients naive to traditional and biologic DMARDs treatment. Rheumatol Int 2016; 36(11): 1579-83.
64. Albano D, Patti C, Lagalla R, Midiri M, Galia M. Whole-body MRI, FDG-PET/CT, and bone marrow biopsy, for the assessment of bone marrow involvement in patients with newly diagnosed lymphoma. J Magn Reson Imaging 2017; 45(4): 1082-9.
65. Gallucci M, Puglielli E, Splendiani A, Pistoia F, Spacca G. Degenerative disorders of the spine. Eur Radiol 2005; 15(3): 591-8.
66. Zha Y, Li M, Yang J. Dynamic contrast enhanced magnetic resonance imaging of diffuse spinal bone marrow infiltration in patients with hematological malignancies. Korean J Radiol 2010; 11(2): 187-94.
67. Muccio CF, Di Blasi A, Esposito G, Brunese L, D'Arco F, Caranci F. Perfusion and spectroscopy magnetic resonance imaging in a case of lymphocytic vasculitis mimicking brain tumor. Pol J Radiol 2013; 78(3): 66-9.
68. De Filippo M, Pesce A, Barile A, Borgia D, Zappia M, Romano A, et al. Imaging of postoperative shoulder instability. Musculoskeletal Surg 2017; 101: 15-22.
69. Zappia M, Castagna A, Barile A, Chianca V, Brunese L, Pouliart N. Imaging of the coracoglenoid ligament: a third ligament in the rotator interval of the shoulder. Skelet Radiol 2017; 46(8): 1101-11.
70. Barile A, La Marra A, Arrigoni F, Mariani S, Zugaro L, Splendiani A, et al. Anaesthetics, steroids and platelet-rich plasma (PRP) in ultrasound-guided musculoskeletal procedures. Br J Radiol 2016; 89(1065).
71. Zappia M, Carfora M, Romano AM, Reginelli A, Brunese L, Rotondo A, et al. Sonography of chondral print on humeral head. Skelet Radiol 2016; 45(1): 35-40.
72. Zappia M, Di Pietto F, Aliprandi A, Pozza S, De Petro P, Muda A, et al. Multi-modal imaging of adhesive capsulitis of the shoulder. Insights Imaging 2016; 7(3): 365-71.
73. Russo A, Reginelli A, Zappia M, Rossi C, Fabozzi G, Cerrato M, et al. Ankle fracture: radiographic approach according to the Lauge-Hansen classification. Musculoskelet Surg 2013; 97 Suppl 2: S155-60.
74. Russo A, Zappia M, Reginelli A, Carfora M, D'Agosto GF, La Porta M, et al. Ankle impingement: a review of multimodality imaging approach. Musculoskelet Surg 2013; 97 Suppl 2: S161-8.
75. Zappia M, Reginelli A, Russo A, D'Agosto GF, Di Pietto F, Genovese EA, et al. Long head of the biceps tendon and rotator interval. Musculoskeletal Surg 2013; 97(suppl. 2): S99-S108.
76. Nurzynska D, DiMeglio F, Castaldo C, Latino F, Romano V, Miraglia R, et al. Flatfoot in children: Anatomy of decision making. Ital J Anat Embryol 2012; 117(2): 98-106.
77. Reginelli A, Pinto A, Russo A, Fontanella G, Rossi C, Del Prete A, et al. Sharp penetrating wounds: spectrum of imaging findings and legal aspects in the emergency setting. Radiol Med 2015; 120(9): 856-65.
78. Miele V, Piccolo CL, Trinci M, Galluzzo M, Ianniello S, Brunese L. Diagnostic imaging of blunt abdominal trauma in pediatric patients. Radiol Med 2016; 121(5): 409-30.
79. Caranci F, Napoli M, Cirillo M, Briganti G, Brunese L, Briganti F. Basilar artery hypoplasia. Neuroradiol J 2012; 25(6): 739-43.
80. Cicala D, Briganti F, Casale L, Rossi C, Cagini L, Cesarano E, et al. Atraumatic vertebral compression fractures: Differential diagnosis between benign osteoporotic and malignant fractures by MRI. Musculoskeletal Surg 2013; 97(suppl. 2): S169-S79.
81. Ilaslan H, Sundaram M. Pediatric and Adult MRI Atlas of Bone Marrow. Normal Appearances, Variants and Diffuse Disease States: Springer; 2016.
82. Minoia C, Maggialetti N, Ferrari C, Brunese L, Rubini G, Guarini A. Can diffusion-weighed whole-body magnetic resonance imaging with body signal suppression play a role in the management of lymphoma patients? J Buon 2016; 21(1): 282-3.
83. Pinto A, Brunese L, Scaglione M, Scuderi MG, Romano L. Gunshot Injuries in the Neck Area: Ballistics Elements and Forensic Issues. Semin Ultrasound CT MRI 2009; 30(3): 215-20.
84. Piccolo CL, Galluzzo M, Trinci M, Ianniello S, Tonerini M, Brunese L, et al. Lower Limbs Trauma in Pediatrics. Semin Musculoskelet Radiol 2017; 21(3): 175-83.
85. Ricci C, Cova M, Kang YS, Yang A, Rahmouni A, Scott WW, Jr., et al. Normal age-related patterns of cellular and fatty bone marrow distribution in the axial skeleton: MR imaging study. Radiology 1990; 177(1): 83-8.
86. Pinto A, Brunese L, Pinto F, Acampora C, Romano L. E-learning and education in radiology. Eur J Radiol 2011; 78(3): 368-71.
87. Briganti F, Delehaye L, Leone G, Sicignano C, Buono G,

Marseglia M, et al. Flow diverter device for the treatment of small middle cerebral artery aneurysms. J Neurointervent Surg 2016; 8(3): 287-94.
88. Caranci F, Tedeschi E, Leone G, Reginelli A, Gatta G, Pinto A, et al. Errors in neuroradiology. Radiol Med 2015; 120(9): 795-801.
89. Reginelli A, Silvestro G, Fontanella G, Sangiovanni A, Conte M, Nuzzo I, et al. Performance status versus anatomical recovery in metastatic disease: The role of palliative radiation treatment. Int J Surg 2016; 33 Suppl 1: S126-31.
90. Pinto A, Reginelli A, Pinto F, Lo Re G, Midiri F, Muzj C, et al. Errors in imaging patients in the emergency setting. Br J Radiol 2016; 89(1061).
91. Iorgulescu JB, Laufer I, Hameed M, Boland P, Yamada Y, Lis E, et al. Benign notochordal cell tumors of the spine: natural history of 8 patients with histologically confirmed lesions. Neurosurgery 2013; 73(3): 411-6.
92. Nishiguchi T, Mochizuki K, Ohsawa M, Inoue T, Kageyama K, Suzuki A, et al. Differentiating benign notochordal cell tumors from chordomas: radiographic features on MRI, CT, and tomography. AJR Am J Roentgenol 2011; 196(3): 644-50.
93. Amano Y, Kumazaki T. Proton MR imaging and spectroscopy evaluation of aplastic anemia: three bone marrow patterns. J Comput Assist Tomogr 1997; 21(2): 286-92.
94. Libicher M, Appelt A, Berger I, Baier M, Meeder PJ, Grafe I, et al. The intravertebral vacuum phenomen as specific sign of osteonecrosis in vertebral compression fractures: results from a radiological and histological study. Eur Radiol 2007; 17(9): 2248-52.
95. Azzali E, Milanese G, Martella I, Ruggirello M, Seletti V, Ganazzoli C, et al. Imaging of osteonecrosis of the femoral head. Acta Biomed 2016; 87 Suppl 3: 6-12.
96. Baur A, Stabler A, Arbogast S, Duerr HR, Bartl R, Reiser M. Acute osteoporotic and neoplastic vertebral compression fractures: fluid sign at MR imaging. Radiology 2002; 225(3): 730-5.
97. McKiernan F, Faciszewski T. Intravertebral clefts in osteoporotic vertebral compression fractures. Arthritis Rheum 2003; 48(5): 1414-9.
98. Madani G, Papadopoulou AM, Holloway B, Robins A, Davis J, Murray D. The radiological manifestations of sickle cell disease. Clin Radiol 2007; 62(6): 528-38.
99. de Divitiis O, Elefante A. Cervical spinal brucellosis: a diagnostic and surgical challenge. World Neurosurg 2012; 78(3-4): 257-9.
100. Spennato P, Rapana A, Sannino E, Iaccarino C, Tedeschi E, Massarelli I, et al. Retropharyngeal cerebrospinal fluid collection as a cause of postoperative dysphagia after anterior cervical discectomy. Surg Neurol 2007; 67(5): 499-503; discussion
101. Muccio CF, Caranci F, D'Arco F, Cerase A, De Lipsis L, Esposito G, et al. Magnetic resonance features of pyogenic brain abscesses and differential diagnosis using morphological and functional imaging studies: A pictorial essay. J Neuroradiol 2014; 41(3): 153-67.
102. Modic MT, Steinberg PM, Ross JS, Masaryk TJ, Carter JR. Degenerative disk disease: assessment of changes in vertebral body marrow with MR imaging. Radiology 1988; 166(1 Pt 1): 193-9.
103. Rahme R, Moussa R. The modic vertebral endplate and marrow changes: pathologic significance and relation to low back pain and segmental instability of the lumbar spine. AJNR Am J Neuroradiol 2008; 29(5): 838-42.
104. Hermann KG, Althoff CE, Schneider U, Zuhlsdorf S, Lembcke A, Hamm B, et al. Spinal changes in patients with spondyloarthritis: comparison of MR imaging and radiographic appearances. Radiographics 2005; 25(3): 559-69; discussion 69-70.
105. McGauvran AM, Kotsenas AL, Diehn FE, Wald JT, Carr CM, Morris JM. SAPHO Syndrome: Imaging Findings of Vertebral Involvement. AJNR Am J Neuroradiol 2016; 37(8): 1567-72.
106. Lubrano E, Marchesoni A, Olivieri I, D'Angelo S, Palazzi C, Scarpa R, et al. The radiological assessment of axial involvement in psoriatic arthritis. J Rheumatol 2012; 39(suppl. 89): 54-6.
107. Spadaro A, Lubrano E. Psoriatic arthritis: imaging techniques. Reumatismo 2012; 64(2): 99-106.
108. Lubrano E, Parsons WJ, Marchesoni A, Olivieri I, D'Angelo S, Cauli A, et al. The definition and measurement of axial psoriatic arthritis. J Rheumatol 2015; 93: 40-2.
109. Falip C, Alison M, Boutry N, Job-Deslandre C, Cotten A, Azoulay R, et al. Chronic recurrent multifocal osteomyelitis (CRMO): a longitudinal case series review. Pediatr Radiol 2013; 43(3): 355-75.
110. Dell'Atti C, Cassar-Pullicino VN, Lalam RK, Tins BJ, Tyrrell PN. The spine in Paget's disease. Skeletal Radiol 2007; 36(7): 609-26.
111. Caranci F, Briganti F, La Porta M, Antinolfi G, Cesarano E, Fonio P, et al. Magnetic resonance imaging in brachial plexus injury. Musculoskeletal Surg 2013; 97(suppl. 2): S181-S90.
112. Jung HS, Jee WH, McCauley TR, Ha KY, Choi KH. Discrimination of metastatic from acute osteoporotic compression spinal fractures with MR imaging. Radiographics 2003; 23(1): 179-87.
113. Dietrich O, Biffar A, Reiser MF, Baur-Melnyk A. Diffusion-weighted imaging of bone marrow. Semin Musculoskelet Radiol 2009; 13(2): 134-44.
114. Nakanishi K, Kobayashi M, Nakaguchi K, Kyakuno M, Hashimoto N, Onishi H, et al. Whole-body MRI for detecting metastatic bone tumor: diagnostic value of diffusion-weighted images. Magn Reson Med Sci 2007; 6(3): 147-55.
115. Schmidt GP, Schoenberg SO, Schmid R, Stahl R, Tiling R, Becker CR, et al. Screening for bone metastases: whole-body MRI using a 32-channel system versus dual-modality PET-CT. Eur Radiol 2007; 17(4): 939-49.
116. Walker R, Kessar P, Blanchard R, Dimasi M, Harper K, DeCarvalho V, et al. Turbo STIR magnetic resonance

imaging as a whole-body screening tool for metastases in patients with breast carcinoma: preliminary clinical experience. J Magn Reson Imaging 2000; 11(4): 343-50.
117. Ierardi AM, Floridi C, Fontana F, Chini C, Giorlando F, Piacentino F, et al. Microwave ablation of liver metastases to overcome the limitations of radiofrequency ablation. Radiol Med 2013; 118(6): 949-61.
118. Elefante A, Peca C, Del Basso De Caro ML, Russo C, Formicola F, Mariniello G, et al. Symptomatic spinal cord metastasis from cerebral oligodendroglioma. Neurol Sci 2012; 33(3): 609-13.
119. Hillengass J, Wasser K, Delorme S, Kiessling F, Zechmann C, Benner A, et al. Lumbar bone marrow microcirculation measurements from dynamic contrast-enhanced magnetic resonance imaging is a predictor of event-free survival in progressive multiple myeloma. Clin Cancer Res 2007; 13(2 Pt 1): 475-81.
120. Palma BD, Guasco D, Pedrazzoni M, Bolzoni M, Accardi F, Costa F, et al. Osteolytic lesions, cytogenetic features and bone marrow levels of cytokines and chemokines in multiple myeloma patients: Role of chemokine (C-C motif) ligand 20. Leukemia 2016; 30(2): 409-16.
121. De Filippo M, Rovani C, Sudberry JJ, Rossi F, Pogliacomi F, Zompatori M. Magnetic resonance imaging comparison of intra-articular cavernous synovial hemangioma and cystic synovial hyperplasia of the knee. Acta Radiol 2006; 47(6): 581-4.
122. Battipaglia G, Avilia S, Morelli E, Caranci F, Perna F, Camera A. Posterior reversible encephalopathy syndrome (PRES) during induction chemotherapy for acute myeloblastic leukemia (AML). Ann Hematol 2012; 91(8): 1327-8.
123. Vassilakopoulos TP, Angelopoulou MK, Constantinou N, Karmiris T, Repoussis P, Roussou P, et al. Development and validation of a clinical prediction rule for bone marrow involvement in patients with Hodgkin lymphoma. Blood 2005; 105(5): 1875-80.
124. Tang YM, Jeavons S, Stuckey S, Middleton H, Gill D. MRI features of bone marrow necrosis. AJR Am J Roentgenol 2007; 188(2): 509-14.
125. De Filippo M, Ingegnoli A, Carloni A, Verardo E, Sverzellati N, Onniboni M, et al. Erdheim-Chester disease: clinical and radiological findings. Radiol Med 2009; 114(8): 1319-29.
126. Piccolo CL, Galluzzo M, Ianniello S, Trinci M, Russo A, Rossi E, et al. Pediatric musculoskeletal injuries: role of ultrasound and magnetic resonance imaging. Musculoskelet Surg 2017; 101(Suppl 1): 85-102.
127. De Filippo M, Corsi A, Evaristi L, Bertoldi C, Sverzellati N, Averna R, et al. Critical issues in radiology requests and reports. Radiol Med 2011; 116(1): 152-62.
128. Nix JS, Fitzgerald RT, Samant RS, Harrison M, Angtuaco EJ. Spinal bone marrow necrosis with vertebral compression fracture: differentiation of BMN from AVN. Skeletal Radiol 2014; 43(9): 1337-40.
129. d'Apuzzo F, Cappabianca S, Ciavarella D, Monsurro A, Silvestrini-Biavati A, Perillo L. Biomarkers of periodontal tissue remodeling during orthodontic tooth movement in mice and men: overview and clinical relevance. ScientificWorldJournal 2013; 2013: 105873.
130. Guarnieri G, Ambrosanio G, Vassallo P, Granato F, Setola FR, Greco B, et al. Combined percutaneous and endovascular treatment of symptomatic aneurysmal bone cyst of the spine: Clinical six months follow-up of six cases. Neuroradiol J 2010; 23(1): 74-84.
131. Briganti F, Marseglia M, Leone G, Briganti G, Piccolo D, Napoli M, et al. Endovascular treatment of a small aneurysm of the superior cerebellar artery with a flow-diverter device. Neuroradiol J 2013; 26 (3): 327-331.
132. Briganti F, Delehaye L, Leone G, Sicignano C, Buono G, Marseglia M, et al. Flow diverter device for the treatment of small middle cerebral artery aneurysms. J NeuroIntervent Surg 2016; 8 (3); 287-294.
133. Briganti F, Tortora F, Elefante A, Volpe A, Bruno MC, Panagiotopoulos K. An unusual case of vertebral arteriovenous fistula treated with electrodetachable coil embolization. Minim Invasive Neurosurg 2004; 47(6): 386-8.
134. Capasso R, Carbone M, Rossi E, Mamone R, Zeccolini R, Reginelli A, et al. A 4-year-old child presenting morning onset of spontaneous tracheal rupture due to bronchial mucous plug occlusion during the nighttime sleep: A case report. J Med Case Rep 2016; 10(1).
135. Cirillo M, Caranci F, Tortora F, Corvino F, Pezzullo F, Conforti R, et al. Structural neuroimaging in dementia. J Alzheimer's Dis 2012; 29 (suppl. 1): 16-9.
136. Daldrup-Link HE, Henning T, Link TM. MR imaging of therapy-induced changes of bone marrow. Eur Radiol 2007; 17(3): 743-61.

Received: 15 September 2017
Accepted: 20 December 2017
Correspondence:
Ferdinando Caranci
Department of Medicine and Health Sciences "V. Tiberio"
University of Molise, via F. De Sanctis 1
86100 Campobasso, Italy
Tel./Fax +39 0817464646;
E-mail: ferdinando.caranci@unimol.it